MID-FIDELITY ANALYSIS OF UNSTEADY INTERACTIONAL AERODYNAMICS OF COMPLEX VTOL CONFIGURATIONS

Davide Montagnani, Matteo Tugnoli, Federico Fonte, Alex Zanotti
davide.montagnani, matteo.tugnoli, federico.fonte, alex.zanotti @polimi.it
Department of Aerospace Science and Technology, Politecnico di Milano, Italy
Monica Syal, Giovanni Droandi
monica.syal, giovanni.droandi @airbus-sv.com
A³ by Airbus LLC, Santa Clara, California, U.S.A.

Abstract

The paper presents a new flexible medium fidelity aerodynamic computational tool, developed from the collaboration between Politecnico di Milano and A³ by Airbus, and tailored to obtain reliable and fast aerodynamic simulations of new aircraft configurations like Vahana, the fully-electric vertical take-off and landing multi-rotor tiltwing aircraft built by A³ by Airbus. The proposed solution, called DUST, relies on the Helmholtz decomposition of the velocity field to recast the aerodynamic problem as a mixed boundary elements-vortex particles method. In DUST different aerodynamic elements can be combined in a single model to best capture the relevant physical phenomena, while an accelerated vortex particle model of the wakes allows for a numerically stable Lagrangian description of the free vorticity evolution. Pressure field evaluation in a rotational flow relies on an integral boundary problem for the Bernoulli polynomial obtained from the Navier–Stokes equation. The code is validated against numerical and experimental data available for conventional vehicle configurations, like airliner and helicopter models, and more complex architechtures, such as a tiltwing-rotor in hover and forward flight. Finally a comparison between flight test data and DUST computations is shown for Vahana.

1 INTRODUCTION

Urbanization and rapidly growing population density are leading to constant increase in traffic. New, safe, fast, reliable, and efficient ways to move around cities are required to complement existing urban transportation systems sustaining commuters needs and better linking cities and regions. A compelling alternative to ground transportation systems in metropolitan areas is represented by Urban Air Mobility, in the form of self-piloted, fully-electric vertical take-off and landing (eVTOL) aircraft.

The design of such eVTOL aircraft demands engineers to predict vehicle performance, stability and handling qualities in many different conditions within the vehicle flight envelope. For instance, during preliminary design a large number of aerodynamic load evaluations are required to explore novel configurations. In a more advanced design phase, a much larger number of aerodynamics analyses are performed to provide loads for sizing the airframe structure and to design and tune the flight control system. As a consequence, computationally efficient and reliable aerodynamic tools are required.

Emerging eVTOLs architectures introduce new aerodynamics challenges as they include in a single vehicle several different features that were usually found separately in conventional airplanes and helicopters. Analyses are further complicated by the fact that many of such architectures undergo some configuration changes during their mission, as for example using tilting wings, nacelles or rotors.

Aerodynamic analysis tools must comply with the needs for building and simulating complex aircraft configurations combining elements with different levels of fidelity, prescribing the motion of an aircraft or some of its components, such as rotors or tilting wings, and providing robust and fast aerodynamic simulations of the flow around the model. High fidelity fluid dynamic computations (CFD) are too computationally expensive to be employed to perform the numerous evaluations required in pre-design phase. Low fidelity aerodynamic tools only provide partial results as they are unable to simulate aerodynamic interactions that characterize new eVTOLs. On the other hand medium

fidelity aerodynamic tools generally provide more reliable results than low fidelity ones and are less computationally expensive than running CFD analysis. However, many of the existing medium fidelity aerodynamic softwares use structured approaches for the wake treatment (panels or filament wakes) that have multiple shortcomings when the wakes interact with bodies or with themselves.

For the above reasons, in order to achieve a quick and reliable estimation of the aerodynamic loads which are robust with respect to the interaction of multiple components and their wakes, new aerodynamic analysis tools must be developed employing a mix of different modelling techniques and fidelity levels.

From the cooperation of A[3] by Airbus and the Department of Aerospace Science and Technology of Politecnico di Milano a new solution has been developed to address these specific requirements. The software is called DUST[8] and is available free under the MIT open source license[9]. The objective of this collaboration is to obtain a flexible and reliable solution to perform aerodynamic simulations of complex eV-TOL vehicles, such as the the Vahana alpha demonstrator pictured in figure 1.

Section 2 of this paper discusses the different modelling methodologies available in DUST and their implementation. In section 3 a selection of application examples of DUST are described and numerical results are compared with experimental and numerical data available for conventional aerodynamic configuration, like airliner models or rotors, and more complex vehicles, such as Vahana. The capabilities of the mix of methodologies employed are shown and the appropriate choices of modelling for different problems are discussed. Finally, in section 4 conclusions are drawn and future developments of DUST currently undergoing are described.

2 METHOD DESCRIPTION

The implementation of DUST exploits the Object Oriented paradigms of the latest Fortran standards to obtain the desired level of flexibility in modelling an aircraft potentially composed of several components and describing their motion. The aerodynamic solver relies on the Helmholtz decomposition of the velocity field, $\vec{u} = \vec{u}_\varphi + \vec{u}_\psi$, being $\vec{u}_\varphi$ and $\vec{u}_\psi$ the irrotational and solenoidal contributions respectively. The solution is advanced in time using a time-stepping algorithm that alternates the solution of a three-dimensional boundary element method for $\vec{u}_\varphi$ and the Lagrangian evolution in time of the rotational part of the velocity $\vec{u}_\psi$. Only the surface mesh of the model is required and different aerodynamic elements allow for different levels of fidelity in the model, ranging from lifting line elements to zero-thickness lifting surfaces and surface panels. Lifting bodies shed a wake from their trailing edges, that can be represented by vortex lattice sheets, vortex particles or a combination of the two.

2.1 Geometry and types of elements

A model can be composed of several components, whose geometry can be imported from CGNS files or defined as parametric components. Each component is associated with a user defined reference frame, whose rigid motion can be prescribed in a hierarchical way, either with respect to the global reference frame or another reference frame. A minimal set of input from the user is needed to automatically define the set of reference frames and motions required to describe stiff or general articulated rotors.

Solid bodies can be represented by a surface mesh of trianglular or quadrilateral surface panels. A piecewise-uniform distribution of doublets and sources is associated to these elements, according to a Morino-like formulation for the velocity potential. Thin lifting bodies can also be modelled as zero-thickness surfaces of vortex lattice elements, for which a velocity based non penetration condition is assigned. The mixed potential-velocity formulation of the boundary element problem results in a linear system whose unknown is the intensity of the doublet distribution on the surface panels and the equivalent doublet intensity of the vortex lattice elements.

One-dimensional lifting line elements can be used to model lifting bodies with high aspect ratio and known aerodynamic characteristics. These elements naturally represent viscous effects, since they rely on tabulated aerodynamic lift, drag and moment coefficients of two-dimensional sections as functions of the relative velocity direction and absolute value. An iterative procedure is used to solve the nonlinear problem of computing the loads on lifting lines, taking into account their mutual interference, using the Kutta-Joukowski theorem to retrieve the circulations of the elements from their lift.

2.2 Wake

Lifting bodies release wakes from the trailing edges that are automatically identified in DUST when loading a general mesh from CGNS files or implied in the parametric definition of a component. Two models of the wake are available in DUST, namely a panel wake and a particle wake, and both can evolve freely or with a rigid prescribed motion. At each timestep, the Kutta condition implemented in the linear system establishes the vorticity balance at the trailing edge and provides the intensity of the first wake panel, while the wake shed by the lifting lines inherits their intensity.

The panel wake consists of a structured set of vortex rings, equivalent to a piecewise uniform distribu-

Figure 1: Vahana (in the front) along with a chase helicopter in a test flight. The final aim of the developed solution is to tackle this complex configuration.

tion of doublets on its surface. Once shed, the circulation associated with the edges of the wake panels keeps a contant value in time. A rigid panel wake allows to obtain reliable results with the least computational effort in simulations of the steady flow around classical configurations, such as airliners, if the wake has a predictable trajectory with limited interactions. A free wake approach produces a more accurate description of wake, with the vertices of the panels convected by the local velocity.

However the structured nature of panel wakes, as well as filament wakes, does not allow them to break when interacting with solid surfaces or other wakes and leads to wake penetrations of the panels. These interactions are responsible for severe numerical instabilities, which in turn lead to a complete degradation of the results. To mitigate this problem several strategies can be adopted to stabilize the solution, however they are heavily dependent on empirical factors and user imputs, leading to debatable results and a significant trial-and-error work overhead for the users.

The vortex particle [2;20] model of the wake was introduced to address this problem in the simulation of the interactional aerodynamics of rotorcraft and complex aircraft configurations. The vortex particles method is a Lagrangian grid-free method that describes the evolution of the wake, through the rotational component of the velocity field $\vec{u}_\psi$, using material vortex particles to obtain the approximate vorticity field,

$$(1) \qquad \vec{\omega}^h(\vec{r}, t) = \sum_{p=1}^{N_p} \vec{\alpha}_p(t) \zeta \left(\vec{r} - \vec{r}_p(t); R_p \right) ,$$

being $\vec{r}_p(t)$ the position, $\vec{\alpha}_p(t)$ the intensity and R_p the radius of the p-th vortex particle, and $\zeta(r)$ the cut-off function that accounts for the distribution of the vorticity induced by each particle. Inserting expression (1)

in the vorticity dynamics equation,

$$(2) \qquad \frac{D\vec{\omega}}{Dt} = \vec{\omega} \cdot \nabla \vec{u} + \nu \nabla^2 \vec{\omega} ,$$

it is possible to obtain the dynamical equations for the intensity $\vec{\alpha}_p(t)$ and the position $\vec{r}_p(t)$ of all the material vortex particles,

$$(3) \qquad \begin{cases} \dfrac{d\vec{\alpha}_p}{dt} = \vec{\alpha}_p \cdot \nabla \vec{u}(\vec{r}_p(t), t) + \nu \text{ “}\nabla^2 \vec{\alpha}_p\text{ “} \\[2mm] \dfrac{d\vec{r}_p}{dt} = \vec{u}(\vec{r}_p(t), t) , \end{cases}$$

to be integrated in time. The term representing the viscosity diffusion " $\nabla^2 \vec{\alpha}_p$ " is computed using the particle strength exchange method (PSE) to approximate the Laplacian operator acting on the vorticity field with an integral operator, as described by Winckelmans [20].

As already mentioned, the mathematical formulation relies on the Helmholtz decomposition of the velocity field $\vec{u} = \vec{u}_\varphi + \vec{u}_\psi$. While the irrotational velocity $\vec{u}_\varphi$ is induced by the free stream velocity, the source, and doublet singularity distributions on the body surface and by the wake panels, the rotational velocity $\vec{u}_\psi$ is induced by the vortex particles. The solenoidal constraint on the rotational velocity, $\nabla \times \vec{u}_\psi = \vec{0}$, allows for the definition of the vector potential $\vec{\psi}$, s.t. $\vec{u}_\psi = \vec{\nabla} \times \vec{\psi}$. This leads to the Poisson's equation for $\vec{\psi}$,

$$(4) \qquad -\nabla^2 \vec{\psi} = \vec{\omega} ,$$

given the gauge condition $\nabla \cdot \vec{\psi} = 0$, the definition of the vorticity field $\vec{\omega} = \nabla \times \vec{u}$ and the vector identity $\nabla \times \vec{u}_\varphi = \nabla \times \nabla \varphi = 0$. The solution of the Poisson's equation (4) reads

$$(5) \qquad \vec{\psi}(\vec{r}, t) = \int_{V_0} G(\vec{r}, \vec{r}_0) \, \vec{\omega}(\vec{r}_0, t) dV_0 ,$$

$$(6) \qquad \vec{u}_\psi(\vec{r}, t) = \int_{V_0} \vec{K}(\vec{r}, \vec{r}_0) \times \vec{\omega}(\vec{r}_0, t) dV_0$$

being $G(\vec{r}, \vec{r}_0)$ the Green's function of the Laplace equation and $\vec{K}(\vec{r}, \vec{r}_0)$ its gradient with respect to the first argument.

Introducing the definition of the particles discretized vorticity field (1) into the equation (6) leads to the equation used to evaluate the contribution of velocity induced by the particles,

$$(7) \qquad \vec{u}_\psi^h(\vec{r}, t) = \sum_{p=1}^{N_p} \vec{K}^h(\vec{r} - \vec{r}_p(t)) \times \vec{\alpha}_p(t) \ .$$

The expression of the discrete kernel $\vec{K}^h(\vec{r} - \vec{r}_p(t))$ must be consistent with the choice of cutoff function ζ. In the singular vortex particle method the cutoff function is equal to a Dirac delta function and the Biot-Savart kernel is retrieved. The choice of the cutoff function ζ made in DUST leads to the Rosenhead-Moore kernel,

$$(8) \qquad \vec{K}^h(\vec{x}, \vec{y}) = -\frac{1}{4\pi} \frac{\vec{x} - \vec{y}}{(|\vec{x} - \vec{y}|^2 + R_v^2)^{3/2}} \ ,$$

a regular kernel that natually fits in the Cartesian fast multipole method (FMM)[1;14] as described in section 2.3. The induced rotational velocity $\vec{u}_\psi$ must be accounted for both in the convection of the material objects and in the right-hand side of the linear system for the potential velocity. Moreover, the gradient of the velocity field is needed to evaluate the vortex stretching-tilting term with the FMM, while this term can be expressed as a function of the vortex intensities and distance between the particles in particle-to-particle interactions[20].

In order to avoid the numerical instabilities occurring with panel wakes, a mixed panel-particle wake or a full particle wake can be employed, by limiting the number of panel rows to a user-defined number or just to the first implicit row.

2.3 Time Evolution

The simulations evolve in time with a time-stepping algorithm in a staggered way. Given the far-field velocity $\vec{U}_\infty$, the motion of the components and the state of the wake at the previous time, the intensity of surface singularities is evaluated. The potential part of the velocity $\vec{u}_\varphi$ is computed with a direct solver as the solution of a linear system, obtained as the discrete counterpart of the mixed kinetic potential-velocity formulation of the aerodynamic problem[12;17]. The linear system is sorted in order to separate the static elements (which do not move and whose influence coefficients do not change) from dynamic elements. The static part is pre-assembled and pre-factorized at the beginning of a simulation, while at each iteration the dynamical part is assembled and the factorization is completed before the system is solved. Lifting line

elements are determined afterwards with an iterative process. The non-linear problem resulting from the use of lookup tables cannot be inserted in the linear system, and is solved with a fixed point algorithm.

The Lagrangian wake evolution step follows. New wake elements are shed, while existing wake elements are convected by the velocity field and the intensity of the vortex particles evolves according to the vorticity equation. The computation of particle interactions is accelerated by the Cartesian FMM and the computational cost is reduced from the $\mathcal{O}(N^2)$ cost of the direct computation of the N particles interaction to the $\mathcal{O}(N)$ cost of the Cartesian FMM evalutation, in the ideal case. An adaptive Octree structure generates a background hierarchical decomposition of the domain into clusters of cells and the interactions between clusters of well separated particles are evaluated with the Cartesian FMM, based on a polynomial representation of the Plummer potential and the Rosenhead kernel. The convergence of the method has been verified to converge to the exact solution with uniformly distributed particles while, in practical cases polynomial orders superior to order 2 led to small or negligible accuracy improvements against a significant increase in the computational costs.

2.4 Pressure and loads

Bernoulli theorems don't hold for rotational flows, as in the case of vortex particle wakes. Even though the Bernoulli polynomial,

$$(9) \qquad B = \frac{|\vec{u}|^2}{2} + \frac{P}{\rho} \ ,$$

is constant throughout the domain, it is possible to compute its value on the surface of the solid bodies as the solution of a boundary integral equation[19]. Taking the divergence of the momentum equation of the incompressible Navier–Stokes' equations leads to the Poisson's problem for B,

$$(10)$$
$$\begin{cases} -\nabla^2 B = \nabla \cdot (\vec{\omega} \times \vec{u}) & \text{in } V \\ B = B_\infty & \text{on } S_\infty \\ \hat{n} \cdot \nabla B = \hat{n} \cdot \left[-\frac{\partial \vec{u}}{\partial t} - \vec{\omega} \times \vec{u} + \nu \nabla^2 \vec{u} \right] & \text{on } S_b \ , \end{cases}$$

with essential boundary conditions at the far field S_∞ and natural boundary conditions on the surface S_b of solid bodies. Manipulating the Poisson's problem using Green's identities, the integral equation for B reads

$$(11) \quad E(\vec{r})B(\vec{r}, t) - \oint_{S_b} \hat{n}(\vec{r}_0, t) \cdot \nabla G(\vec{r}, \vec{r}_0)B(\vec{r}_0, t) =$$
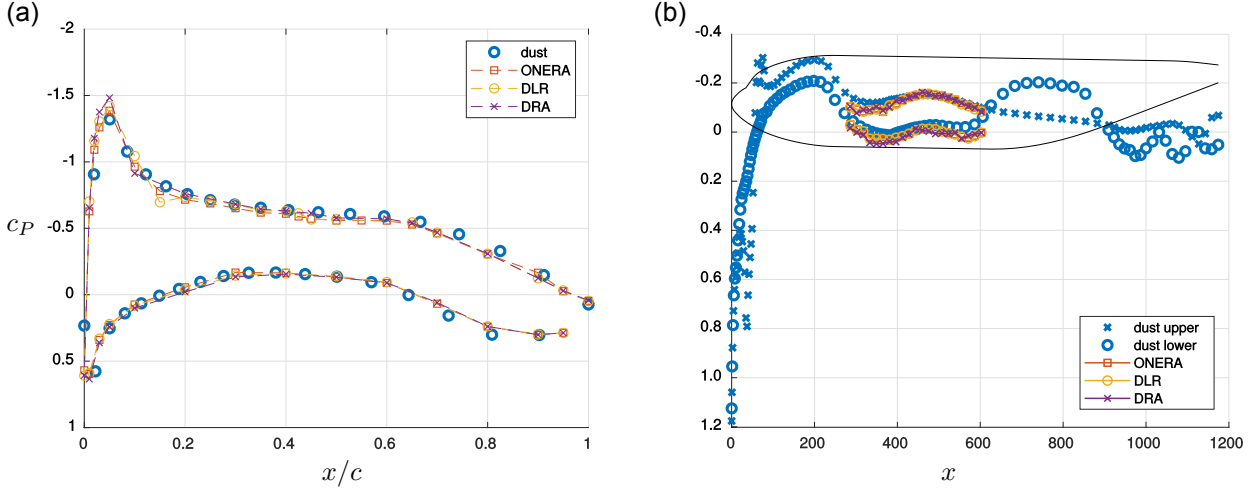
(a)

(b)

Figure 2: DLR-F4 model. (a) Pressure coefficient c_P on the wing section at $\eta = 2y/b = 0.636$. (b) Pressure coefficient on the fuselage in the symmetry plane. Comparison of the compressible potential results with the experimental results[18].
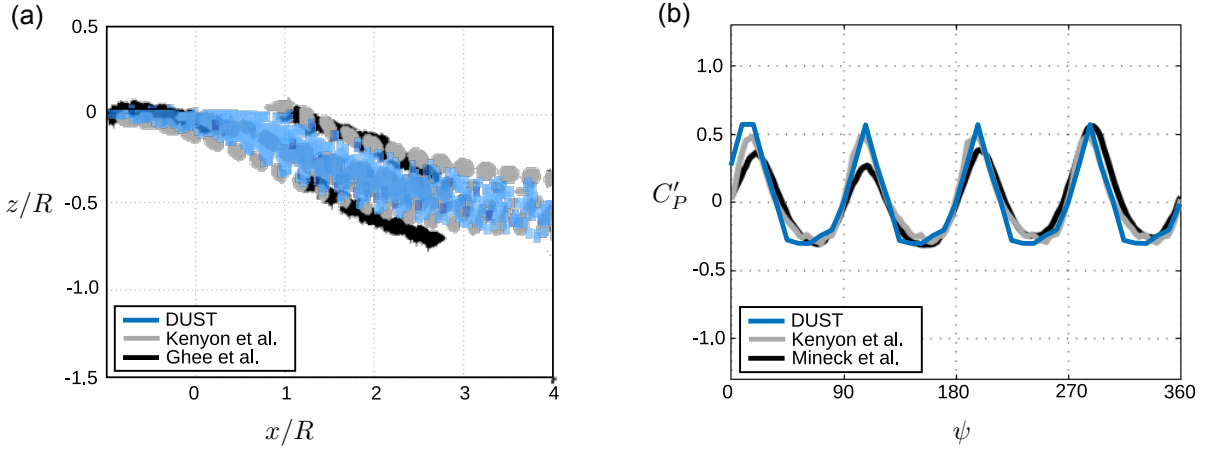
(a)

(b)

Figure 3: ROBIN model. (a) Wake evolution in forward flight at $\mu = 0.15$, $c_T = 0.0065$. Vortex particles from DUST compared with VTM results from Kenyon and Brown[13] and flow visualisation of Ghee et al.[11]. (b) Modified pressure coefficient C'_P in a probe located on centerline of the fuselage $x/R = 0.2$ far from the nose of the fuselage compared with the numerical results from Kenyon and Brown[13] and the experimental measurements of Mineck and Althoff Gorton[16].

$$
\begin{aligned}
&= B_\infty + &\text{(free stream)}\\
&+ \oint_{S_b} G(\vec{r}, \vec{r}_0)\hat{n}(\vec{r}_0, t) \cdot \frac{\partial \vec{u}}{\partial t}(\vec{r}_0, t) + &\text{(unsteady)}\\
&+ \oint_V \nabla G(\vec{r}, \vec{r}_0) \cdot \vec{\omega}(\vec{r}_0, t) \times \vec{u}(\vec{r}_0, t) + &\text{(rotational)}\\
&+ \oint_{S_b} G(\vec{r}, \vec{r}_0)\hat{n}(\vec{r}_0, t) \cdot \nabla^2 \vec{u}(\vec{r}_0, t) \, , &\text{(viscous)}
\end{aligned}
$$

where $E(\vec{r}) = 1/2$ on the boundary of the domain. For moving bodies, the partial derivative $\partial \vec{u}/\partial t$ is related to the time derivative of the velocity on the surface panels,

$$
(12) \qquad \left.\frac{\partial \vec{u}}{\partial t}\right|_b = \frac{\partial \vec{u}}{\partial t} + \vec{u}_b \cdot \nabla \vec{u} \, ,
$$

where $\vec{u}_b$ is the velocity of the body and the required spatial derivatives on the surface are computed with the Constrained Hermite Taylor Series Least Square (CHTLS) method[15]. The viscous contributions to the Bernoulli polynomial is neglected. The discrete counterpart of the integral equation (11) is a linear system with the same matrix as the one already computed to solve for the doublet intensity of the panels, except for the Kutta condition. If the model has no moving components modelled with surface panels, also this matrix is assembled and factorized just once.

On lifting lines the loads are retrieved from the lookup tables and contain both the pressure and viscous contributions, while on the rest of the elements the loads contain only the pressure contribution. More complex methods to simulate viscous contributions on surface panels are currently under development.
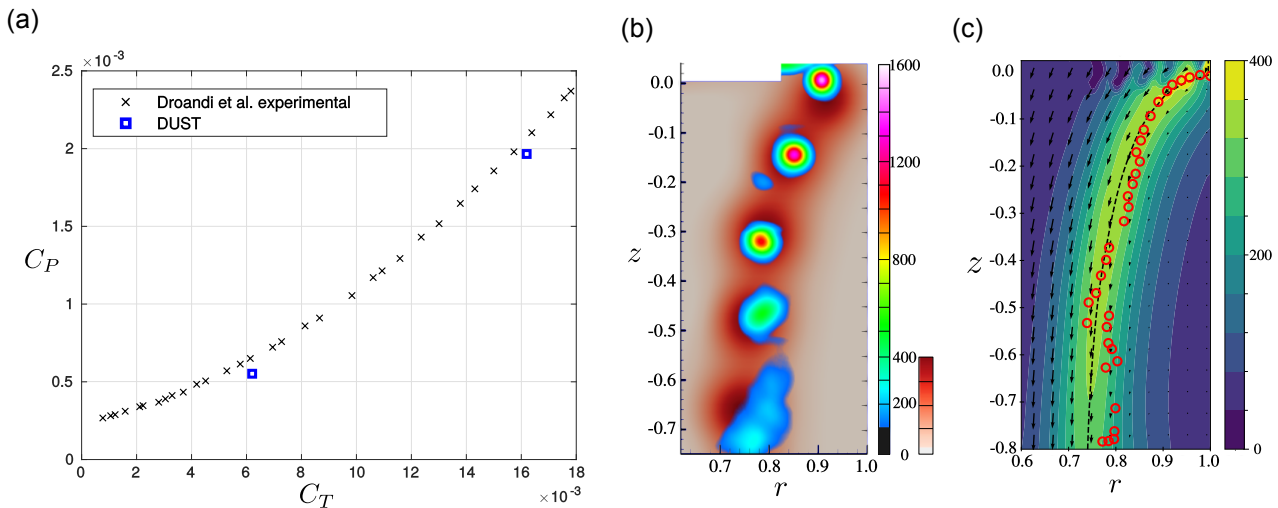
Figure 4: Isolated rotor in hover. (a) Power coefficient C_P as a function of net thrust coefficient C_T in hover. (b) Phase-average out-of-plane vorticity field $\omega_\theta(r, z)$ in an azimuthal plane below the rotor. The experimental measurements of the core of the tip vortexes are compared to the computed vorticity field, shown with a white-to-red colormap: the results of experiments are shown in the regions where $|\omega_\theta| > 100\,s^{-1}$. (c) Averaged maps of vorticity $\omega_\theta(r, z)$. Arrows: direction of the average velocity field. Dashed line: radial coordinate of the maximum of the vorticity field. Red circles: vortices cores position from PIV measurement of Droandi et al.[5].

3 NUMERICAL RESULTS

In this section, a selection of application examples analyzed with DUST is presented, spanning different configurations to demonstrate the flexibility of DUST and to help the discussion about the best modelling choices for the components of a complex aircraft configurations.

3.1 Wing-Fuselage Interaction

The compressible subsonic flow around a conventional aircraft configuration is studied using a standard panel method with both rigid and free models of the wake. The wing-fuselage interaction is validated against the subsonic experimental data available for the DLR-F4 model, used in the 1st AIAA Drag Reduction Workshop[18]. The free stream Mach number is $M_\infty = 0.6$ and Prandtl-Glauert correction implemented in DUST manages to represent the compressibility effects on the pressure coefficient, as shown in figure 2 with the distribution of the pressure coefficient on a wing section and in the symmetry plane along the fuselage.

In this case, the topology and the predictable evolution of the wake without strong interactions with the body makes a free panel wake, or even a rigid panel wake, the best choice to predict the steady loads on the airplane with the minimal computational effort.

3.2 Rotor-Fuselage Interaction

The rotor-fuselage interaction problem is investigated taking into account the well known ROBIN fuselage geometry[16;10], equipped with a four-bladed fully articulated 3.15 m diameter single rotor. The fuselage is modelled with three dimensional surface panels, while lifting lines blades and full particle wake are used in order to retrieve the viscous contribution of torque and required power from a stable aerodynamic simulation of the model, avoiding any numerical instability despite the strong wake-to-wake and wake-to-fuselage interactions. The analysed flight condition is a levelled forward flight with advance ratio $\mu = 0.15$ and thrust coefficient $c_T = 0.0065$. The results obtained with DUST presented in figure 3 show a good agreement in the comparison with the available numerical results of Kenyon and Brown[13] and the experimental measurements of Ghee et al.[11] and Mineck and Althoff Gorton[16], in terms of wake evolution and modified pressure coefficient on the fuselage,

$$C_P' = 100\frac{P - P_\infty}{\frac{1}{2}\rho(\Omega R)^2} \ .$$

3.3 Wing-Rotor interaction

The code is further validated against the results of the experimental activities performed in the open test section of the Politecnico di Milano wind tunnel on a tiltwing-rotor model, reproducing different flight conditions and aircraft configurations. The model is composed of a four-blade rotor[3] rotating around a nacelle, at the tip of the tilting section of a half-span
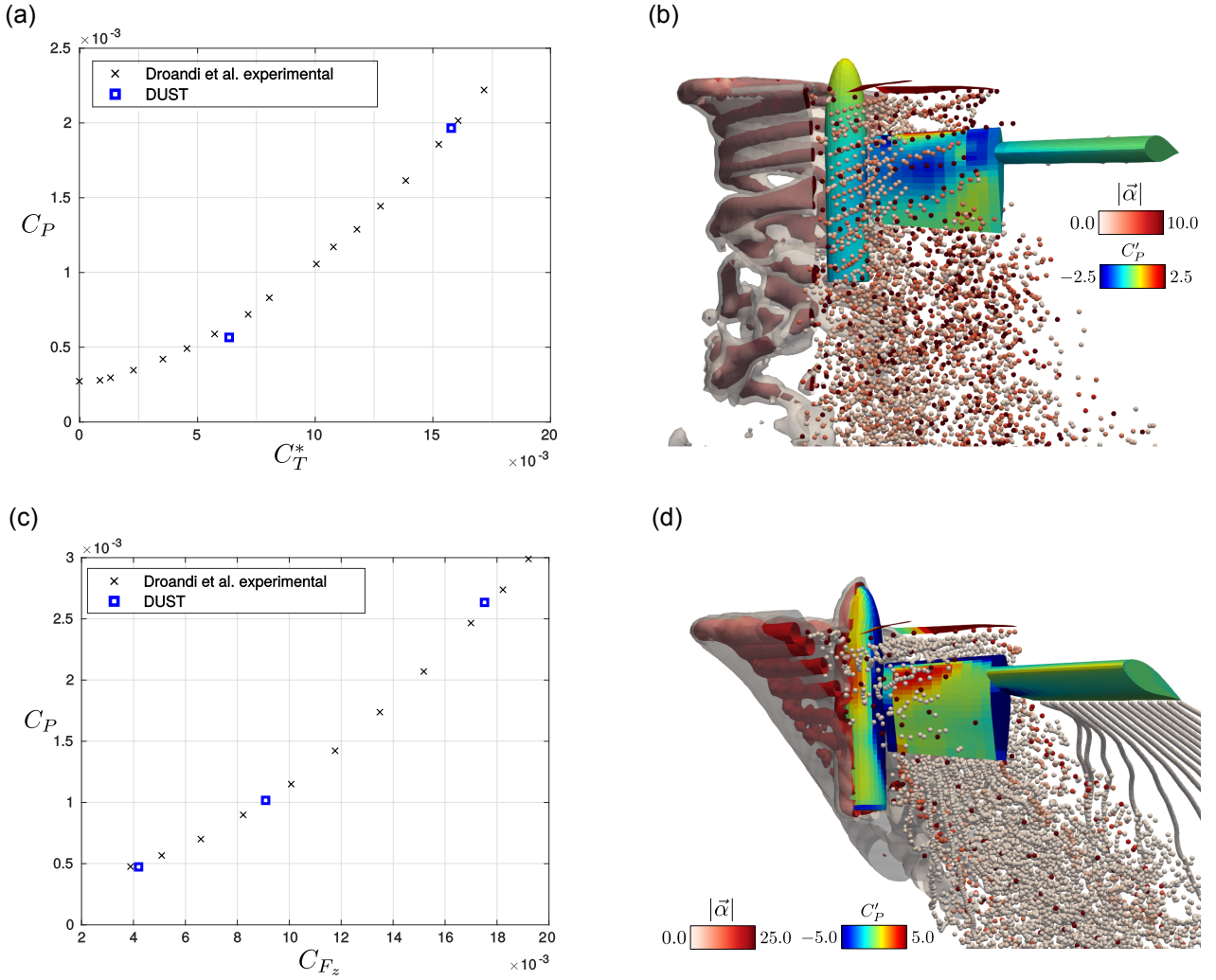
(a)

(b)

(c)

(d)

Figure 5: Rotor-wing model in hover and forward flight. Hover: (a) power coefficient C_P as a function of net thrust coefficient C_T^*; (b) pressure coefficient C_P' on the body and visualization of the flow field with the vortex particle distribution of intensity $|\vec{\alpha}|$ and iso-surfaces of the vorticity magnitude, at $C_T^* = 1.54 \cdot 10^{-2}$. Forward flight, with advance ratio $\mu = 0.115$: (c) power coefficient C_P as a function of rotor vertical force coefficient C_{F_z}; (d) visualization of the flow field with the vortex particle distribution and vorticity iso-surfaces, at $C_{F_z} = 9.10 \cdot 10^{-3}$. Iso-contours of the vorticity field magnitude corresponding to $\widetilde{\omega} = 5.0$ and 7.0 are shown in grey and red, respectively.

wing[5].

The rotor blades are modelled as lifting lines, while the nacelle and the wing are modelled with surface panels to effectively capture the interactions of the wake with the solid bodies.

The isolated rotor model is analysed in hover condition (tip Mach number equal to 0.32, collective pitch equal to 12°). Rotor performance and the shape of the wake obtained with DUST are compared with the available load cells and PIV measurements respectively. In figure 4(a) the thrust and power coefficient are presented, showing a fair agreement with the experimental data. In figure 4(b) the phase-averaged vorticity component orthogonal to an azimuthal plane shows a good matching between the numerical and experimental results, both for the position and the in-

tensity of the blade tip vortices. The time-averaged vorticity field represented in figure 4(c) confirms that the particle wake accurately represents the contraction of the wake and the downwash produced by the rotor.

The tiltwing-rotor configuration is analysed coupling the half span partially tilting wing with the rotor model. In hover flight condition the outer portion of the wing is rotated vertically by 90° and aligned with the rotor axis. In figure 5(a), torque versus net thrust show a good agreement of the integral loads with the experimental measurements[4], while figure 5(b) depicts the evolution of the wake interacting with the solid bodies without penetration or instabilities.

Good agreement between numerical results and experiments[6] is also found analysing the tiltwing-rotor

model in forward flight, at the beginning of a conversion manoeuvre, with the rotor, the nacelle and the outer portion of the wing tilted by 75°. The numerical results are presented in figure 5(c,d) and closely match the experimental results. The intensity $\widetilde{\omega}$ of non-dimensional vorticity fields shown in this section are scaled using the rotor radius and its period as the reference scales of length and time. Particle intensity is further scaled using the volume of the vortex particles.

3.4 Full Vehicle Configuration

The aerodynamics of Vahana is strongly influenced by interactions between the wings, the rotors and their wakes. Such phenomena need to be properly simulated in order to predict and improve the handling qualities and the performance of the vehicle throughout the flight envelope.

The numerical model of the vehicle is composed of several components: the fuselage, the tilting canard and wing, and three blades per rotor. Fuselage, canard, and wing are modelled with three dimensional surface panels in order to capture the interactions of the particle wake with them. Rotor blades are modelled as lifting lines.

Vehicle angle of attack, canard and wing tilt angles, rotational speed of the rotors and collective pitch setting of the rotor blades taken from the flight test measurements are provided to DUST as the input of the numerical model. In the following, numerical simulations are compared with flight test data. The integral loads acting on the aircraft are computed and used to check the vehicle trim at each flight condition analysed. The intensity $\widetilde{\omega}$ of non-dimensional vorticity fields shown in this section are scaled using the fan radius and the period of the canard fans as the reference scales of length and time. Particle intensity is further scaled using the volume of the vortex particles. Two trimmed flight conditions are studied: hover and forward flight at $V = 36.5\,m/s$. For more deteils and previous analysis on similar configurations see Droandi et al.[7].

In hover, the fuselage pitch angle is nearly equal to zero, the wings are tilted vertically and the rotors have similar rotational speeds. In this flight condition, the canard and the wing are fully immersed in the wake of their fans. The initial coherence of the tip vortices and the axial symmetry of the wake of each rotor are partially lost downstream because of the strong interactions with both the body surface and the wake shedded by the neighboring fans, as shown in figure 6. It is also possible to observe how the wake of a rotor installed on the canard, which are slightly tilted forward, is then deflected forward by the canard itself.

The predicted loads show a good agreement with the measurements performed during the flight tests. The difference with the trim conditions during the flight

test are reported in table 1, in terms of the relative error on the lift,

$$(13) \qquad \frac{\Delta L}{Q} = \frac{L^{DUST} - Q}{Q} \, ,$$

and the relative error in the longitudinal position of the point of application of the aerodynamic forces,

$$(14) \qquad \frac{\Delta x_a}{c} = \frac{x_a^{DUST} - x_a^{TRIM}}{c} \, ,$$

being L the computed lift, Q the weight of the aircraft, c the canard reference chord, x_a^{DUST} the longitudinal position of the point of application of the aerodynamic forces computed with DUST and x_a^{TRIM} the position ensuring pitch trim.

The second trim condition analysed corresponds to a forward flight speed of $36.5\,m/s$ and is characterized by small canard and wing tilt angles and non-zero blade collective pitch setting. Differential thrust produced by rotors spinning at slightly different speeds allows to trim the vehicle with a small positive angle of attack. In this flight condition, the wakes of the fans weakly interact with solid bodies and neighboring fans, while the wakes shed by the canard and its fans directly influence the inflow on the wing fans, as they are convected downstream. Figure 7(a) shows the wake systems, along with the pressure coefficient,

$$(15) \qquad C_P = \frac{P - P_\infty}{\frac{1}{2}\rho U_\infty^2} \, ,$$

on the solid surface of the model. The helical vortex structures shed by the tip of the rotor blades preserve their regular structure along the whole computational domain. The helical structures weakly affect the tip vortex released from the upper winglets, while stronger interactions lead to the instability of the canard tip vortices. The average inflow velocity on the fan disks are presented in figure 7(b) in terms of the non-dimensional inflow velocity,

$$(16) \qquad w = \frac{(\vec{u} - \vec{U}_\infty) \cdot \hat{z}_{axis}}{V_{TIP}^c} \, ,$$

where $\vec{u}$ is the velocity on the rotor disk, $\vec{U}_\infty$ is the free stream velocity, $\hat{z}_{axis}$ the unit vector normal to the plane of the rotor and V_{TIP}^c the tip velocity of the canard fans. The footprint of the canard fans result in a region of accelerated flow in the lower part of the wing fan disk, while the blockage effect of the fuselage can be observed on the canard inboard fan. The vertical trim is reached within a relative error of 1.0% reducing the vehicle angle of attack of $1.1°$ with respect to the experimental measurements performed during the flight test campaign. Using this vehicle angle of attack, the numerical results are close to match the pitch trim conditions as well, as reported in table 1.
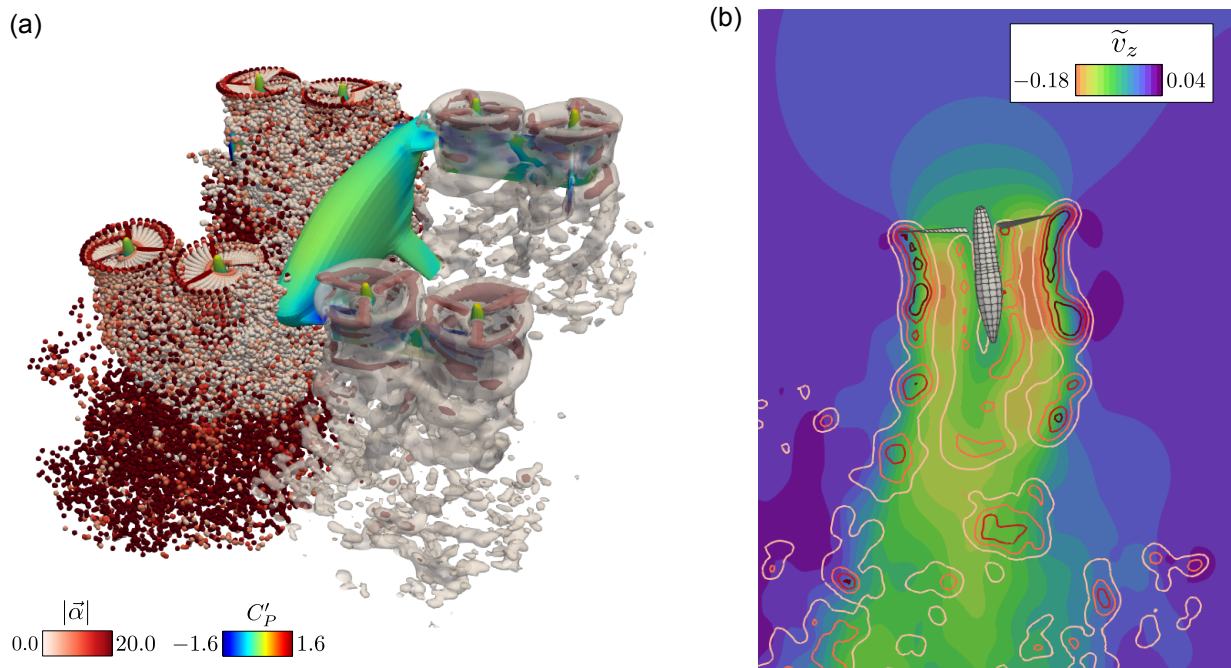
(a)

(b)

Figure 6: Vahana in hover condition. (a) Pressure coefficient C'_P on the body and visualization of the wake with the vortex particle distribution of intensity $|\vec{\alpha}|$, on the right side, and iso-contours of the vorticity field magnitude corresponding to $\widetilde{\omega} = 1.82$ (grey) and $\widetilde{\omega} = 4.17$ (red), on the left side. Particle lumping far from the rotors results in a reduction of the numbers of particles and an increase of their intensity, as can be observed in the left side of the figure. (b) Instantaneous non-dimensional vertical component $\widetilde{v}_z = v_z/V^c_{TIP}$ of the velocity field $\vec{v}$ and contour levels of the vorticity field $\widetilde{\omega} = 1 : 4$, from white to red, in the plane parallel to the plane of symmetry of the aircraft, passing through the vertex of the nacelle of the canard outboard fan.

	$\Delta L/Q$	$\Delta x_a/c$
Hover	$-8.4 \cdot 10^{-3}$	$4.7 \cdot 10^{-2}$
Late transition	$1.0 \cdot 10^{-2}$	$2.3 \cdot 10^{-2}$

Table 1: Vertical and pitch trim conditions. Comparison between the numerical results and the flight test data.

4 CONCLUSIONS

A new mid-fidelity computational tool, called DUST, is presented in this paper. The tool aims at meeting the need for fast aerodynamic simulations in the design of modern eVTOL configurations, like the Vahana alpha demonstrator by A^3 by Airbus. The elements used to represent solid bodies, ranging from lifting lines to three-dimensional surface panels, allow for different levels of fidelity in the model. A panel wake model ensures low computational costs in classical aeronautical configurations, while a vortex particle model provides a numerically stable description of the wakes, even when strong wake-body interactions characterize the flow around the aircraft configuration analyzed. The evaluation of particles interactions is accelerated using a Cartesian Fast Multipole algorithm. The pressure field is retrieved by solving a Poisson's problem for the Bernoulli polynomial.

First, the implemented methods are verified on conventional aircraft and helicopter configurations. Then, the heavy interactional flow around a tiltwing-rotor model is simulated and the results obtained with DUST are successfully compared with the experimental results.

Finally the full Vahana alpha configuration is analyzed. Despite its limitations in predicting viscous stress contributions and flow separations, the numerical simulations performed with DUST are in good agreement with the flight test data of Vahana, in terms of trim conditions.

Ongoing research activities involve the study of viscous effects, with the fundamental goal of integrating the current status of the code with the estimation of viscous stresses and a diffused release of vorticity from smooth surfaces to simulate flow separations.

References

[1] R. E. Brown and A. J. Line. Efficient high-resolution wake modeling using the vorticity
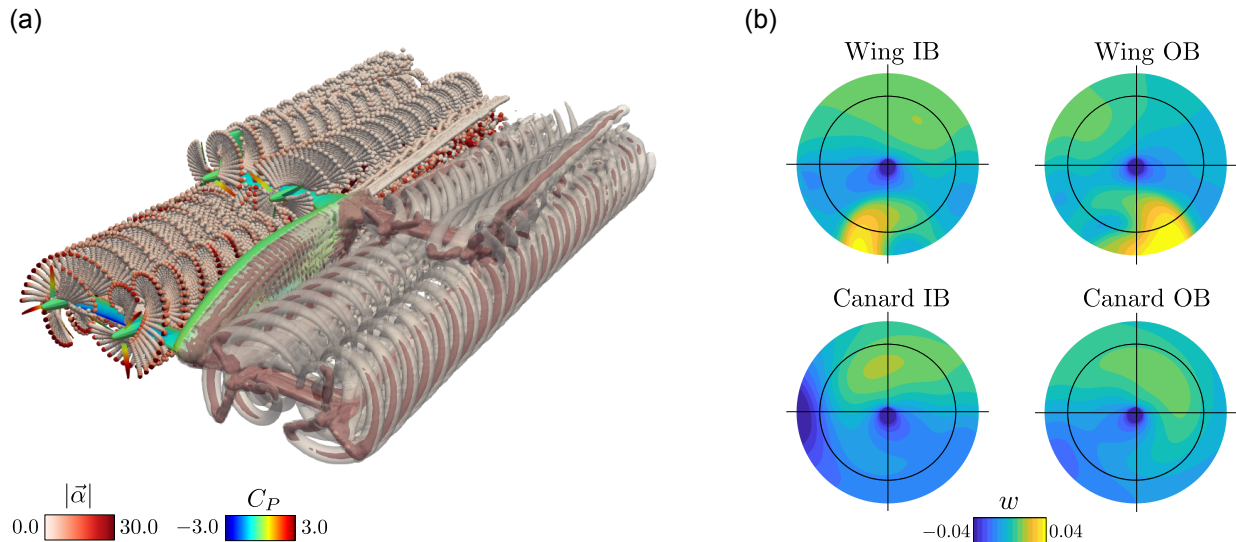
Figure 7: Vahana in forward flight. (a) Pressure coefficient C_P on the body and visualization of the wake with the vortex particle distribution of intensities $|\vec{\alpha}_p|$, on the right side, and iso-contours of the vorticity field magnitude corresponding to $\widetilde{\omega} = 0.78$ (grey) and $\widetilde{\omega} = 1.95$ (red), on the left side. (b) Maps of the non-dimensional inflow velocity w on the rotor disks: average value over two revolutions. Black circles represent the rotor disk of the fans.

transport equation. *AIAA Journal*, 43(7):1434–1443, 2005.

[2] G.-H. Cottet, P. D. Koumoutsakos, D. Petros, et al. *Vortex methods: theory and practice*. Cambridge University Press, 2000.

[3] G. Droandi and G. Gibertini. Aerodynamic blade design with multi-objective optimization for a tiltrotor aircraft. *Aircraft Engineering and Aerospace Technology: an International Journal*, 87(1):19–29, 2015.

[4] G. Droandi, G. Gibertini, A. Zanotti, D. Grassi, and G. Campanardi. Experimental investigation of the rotor-wing aerodynamic interaction in a tiltwing aircraft in hover. *The Aeronautical Journal*, 119(1215):591–612, 2015.

[5] G. Droandi, A. Zanotti, and G. Gibertini. Aerodynamic interaction between rotor and tilting wing in hovering flight condition. *Journal of the American helicopter Society*, 60(4):1–20, 2015.

[6] G. Droandi, G. Gibertini, D. Grassi, G. Campanardi, and C. Liprino. Proprotor–wing aerodynamic interaction in the first stages of conversion from helicopter to aeroplane mode. *Aerospace Science and Technology*, 58:116 – 133, 2016.

[7] G. Droandi, M. Syal, and G. Bower. Tiltwing multi-rotor aerodynamic modeling in hover, transition and cruise flight conditions. In *Proceedings*

of the 74th Annual Forum, Phoenix, May 2018. AHS International.

[8] DUST - an aerodynamics solution for complex configurations.
URL: https://www.dust-project.org/.

[9] DUST repository.
URL: https://gitlab.com/dust_group/dust.

[10] C. E. Freeman and R. E. Mineck. Fuselage surface pressure measurements of a helicopter wind-tunnel model with a 3.15-meter diameter single rotor. Technical Report 80051, NASA Langley Research Center, March 1979.

[11] T. A. Ghee, J. D. Berry, L. A. Zori, and J. W. Elliott. Wake geometry measurements and analytical calculations on a small-scale rotor model. Technical Report TP 3584, NASA, 1996.

[12] J. L. Hess. Calculation of potential flow about arbitrary three-dimensional lifting bodies. Technical report, Douglas Aircraft Co., Long Beach CA, 1972.

[13] A. R. Kenyon and R. E. Brown. Wake dynamics and rotor-fuselage aerodynamic interactions. *Journal of the American Helicopter Society*, 54(1):12003–12003, 2009.

[14] K. Lindsay and R. Krasny. A particle method and adaptive treecode for vortex sheet motion in three-dimensional flow. *Journal of Computational Physics*, 172(2):879–907, 2001.

[15] R. A. McDonald and A. Ramos. Constrained Hermite interpolation for mesh-free derivative estimation near and on boundaries. *AIAA Journal*, 49(10):2248–2257, 2011.

[16] R. E. Mineck and S. Althoff Gorton. Steady and periodic pressure measurements on a generic helicopter fuselage model in the presence of a rotor. Technical Report NASA/TM-2000-210286, Langley Research Center, Hampton, Virginia, 2000.

[17] L. Morino and C.-C. Kuot. Subsonic potential aerodynamics for complex configurations: a general theory. *AIAA Journal*, 12(2):191–197, 1974.

[18] G. Redeker and R. Müller. *A comparison of experimental results for the transonic flow around the DFVLR-F4 wing body configuration*. DFVLR, 1985.

[19] J. S. Uhlman. An integral equation formulation of the equations of motion of an incompressible fluid. Technical report, NAVAL UNDERSEA WARFARE CENTER DIV NEWPORT RI, 1992.

[20] G. S. Winckelmans. *Topics in vortex methods for the computation of three-and two-dimensional incompressible unsteady flows*. PhD thesis, California Institute of Technology, 1989.